

Tunable Linear Polarization-State Generator of Single Photons on a Lithium Niobate Chip


Jiafan Wu¹,[✉] Yiwen Huang,¹ Chuanyi Lu¹,[✉] Tingting Ding,¹ Yuanlin Zheng^{1,2,*} and Xianfeng Chen^{1,2,3,4,†}

¹State Key Laboratory of Advanced Optical Communication Systems and Networks, School of Physics and Astronomy, Shanghai Jiao Tong University, Shanghai 200240, China

²Shanghai Research Center for Quantum Sciences, Shanghai 201315, China

³Jinan Institute of Quantum Technology, Jinan 250101, China

⁴Collaborative Innovation Center of Light Manipulation and Applications, Shangdong Normal University, Jinan 250358, China

 (Received 10 March 2020; revised manuscript received 4 May 2020; accepted 26 May 2020; published 29 June 2020)

Controlling the polarization state of light at a fast speed is important in both classical and quantum regimes. Here, we present an easily integrated compact tunable linear polarization-state generator of single photons in the telecom wavelength band on a periodically poled lithium niobate on insulator (PPLNOI) chip. The linear polarization of single photons can be continuously rotated by applying a transverse electric field utilizing the electro-optic (EO) effect. With strong light confinement and the large EO coefficient in the PPLNOI ridge waveguide, dramatically reduced driving voltage and fast-speed modulation is realized. Moreover, quantum entanglement is well maintained during the switching of polarization states, as proved in the time-energy entanglement measurement. The scheme holds promise for realizing integrated quantum optics.

DOI: [10.1103/PhysRevApplied.13.064068](https://doi.org/10.1103/PhysRevApplied.13.064068)

I. INTRODUCTION

Quantum-information science is a rapidly developing field of interdisciplinary research, which is closely related to quantum mechanics and information theory. Over the last decades, quantum photonics has become a thriving research field, promoting both fundamental investigation of quantum phenomena and applied quantum technologies [1,2]. However, complex quantum-optics solutions implemented in bulk optics have serious drawbacks, such as integration difficulty, conversion inefficiency, and stability weakness. An effective approach to overcome these limitations is to adopt photonic integrated circuits, e.g., waveguide structures, which offer many advantages compared to bulk optics. The emerging technology of lithium niobate on insulator (LNOI) [3] has provided an ideal platform for such a purpose, and enabled a variety of important functionalities, such as compact single-photon sources [4,5], quantum memories [6,7], and single-photon frequency conversion [8,9].

Fast and precise controlling of the polarization of individual photons has been essential in polarization-entangled photon sources [10–12], quantum communication [13,14],

as well as quantum computing [15]. Recently, a variety of progresses have been achieved in single-photon polarization control techniques [16–18], providing a solid strategy for high-performance quantum-information processing. However, based on phase retardation between o- and e-polarized waves in electro-optic bulk media, the case is that linear polarization is only preserved in a set of orthogonal directions, e.g., vertical and horizontal states. As for other directions, the output polarization is either elliptical or circular. Access to pure linearly polarized single photons is critical for various applications. For example, the proposed quantum-computer applications rely on photons with distinct energy and polarization vectors. In addition, a common requirement raised for several optoelectronic applications, e.g., (bio)dermatology [19], optical quantum computers, is also in need of linearly polarized light for their operation. Moreover, fully linearly polarized single photons can also be used to realize multibase vector quantum key distribution. Therefore, it is crucial to keep single photons fully linearly polarized while maintaining their quantum characteristics during the polarization control.

Here, we report on the manipulation of single photons' polarization in a periodically poled lithium niobate on insulator (PPLNOI) ridge waveguide at the telecommunication wavelength, while preserving their

*ylzheng@sjtu.edu.cn

†xfchen@sjtu.edu.cn

fully linear polarization characterization. In this configuration, we demonstrate the rotation of single photons' linear polarization through the transverse electro-optic (EO) effect, with the advantages of integration, low drive voltage, as well as fast-speed response. Their quantum characteristics is maintained after the polarization control, as shown in the time-energy entanglement measurement. Combined with previously demonstrated manipulation of single photons' amplitude [20], frequency [8,9], path [16], and phase [21,22], the fast linearly polarization control scheme described here can add to the complete control of single photons.

II. THEORY AND EXPERIMENT

In our scheme, the control of the polarization state is achieved using a PPLNOI ridge waveguide (HC Photonics, Co.). The cross-section view of the PPLNOI ridge waveguide is sketched in Fig. 1(a), whose dimension is $6.0 \mu\text{m}$ (width) $\times 5.0 \mu\text{m}$ (height) $\times 10 \text{mm}$ (length). The ridge waveguide located between two parallel $2.5\text{-}\mu\text{m}$ deep grooves is fabricated using optical grade dicing on a chemomechanically thinned PPLN layer ($5.0 \mu\text{m}$ thick) [23,24]. The poling period, Λ , of the PPLN is $20.5 \mu\text{m}$ with a duty cycle of 50%, which is designed to fulfill quasi-phase matching (QPM) in the telecommunication band. The optical axis is along the z axis. With high refractive-index contrasts, light transmitted along the x axis of the ridge waveguide can be strongly confined. Then, a metal (Ni or Cr) electrode is deposited on both side walls to form the transverse electrode.

The TE \leftrightarrow TM mode conversion mechanism in the PPLNOI ridge waveguide is similar to that in bulk PPLN experiencing transverse EO effect [25]. When a transverse (y -axis) electric field is applied along the PPLN crystal, the optical axes of each of the positive and negative domains are alternately rearranged at small rocking angles of θ and $-\theta$ about the x axis. The deviation angle θ is proportional to the applied electric field intensity, E , and has the form of $\theta \approx \gamma_{51}E/[(1/n_e)^2 - (1/n_o)^2]$, where γ_{51} is the EO coefficient, and n_e , n_o are the extraordinary and ordinary refractive indices, respectively. Meanwhile, the operating wavelength satisfying the QPM condition is given by $\lambda = \Lambda(n_o - n_e)$, and is consequently temperature

dependent, where Λ is the period of PPLN. Therefore, the operating wavelength can be adjusted by temperature control. At the QPM wavelength, the output polarization is rotated by an angle of $2N\theta$ with respect to its horizontal or vertical initial state, where N is the number of domains that the optical wave propagates through. Notably, the linear polarization state of light remains in this configuration, which makes QPM PPLN an actual linear polarization rotator or generator.

Using quantum theory, the physics of our experiment can be described by the following effective Hamiltonian [20]:

$$\hat{H} = i\hbar(\chi E_p \hat{a}_{sH}^+ \hat{a}_{sV} - \text{H.c.}), \quad (1)$$

where E_p is the electric-field amplitude of pump lasers, and \hat{a}_s (\hat{a}_s^+) is the annihilation (creation) operator for the wave at frequency ω_s , where s represents signal photons. H and V represent the quantum polarization states in the horizontal and vertical directions, respectively. $\chi = \gamma_{51}f(x)\omega_s E_y/(2c) \times \sqrt{n_{sy}^3 n_{sz}^3} e^{i\Delta k_{EO}x}$ is the coupling coefficient, where E_y , n are the transverse electric field amplitude and refractive index, respectively. c is the speed of light in vacuum, and ω denotes angular frequency. $f(x)$ is the structural function of PPLN, and it can be written as Fourier series: $f(x) = \sum_m g_m \exp(-iG_m x)$, where $G_m = 2m\pi/\Lambda$ is the reciprocal lattice vector (m is the order of QPM). g_m is the amplitude of reciprocal lattice vector. $\Delta k_{EO} = k_{sV} - k_{sH}$ is the phase mismatch of the EO polarization coupling process. H.c. denotes a Hermitian conjugate. Using the Heisenberg equation of motion, the coupled mode equations describing the EO process can be obtained from Eq. (1):

$$\frac{d\hat{a}_{sH}}{dt} = \chi E_p \hat{a}_{sV}, \quad (2a)$$

$$\frac{d\hat{a}_{sV}}{dt} = -\chi^* E_p^* \hat{a}_{sH}. \quad (2b)$$

Equation (2) indicates that the linear polarization state of single photons can be controlled by the EO effect, specifically, by the applied voltage on the PPLN.

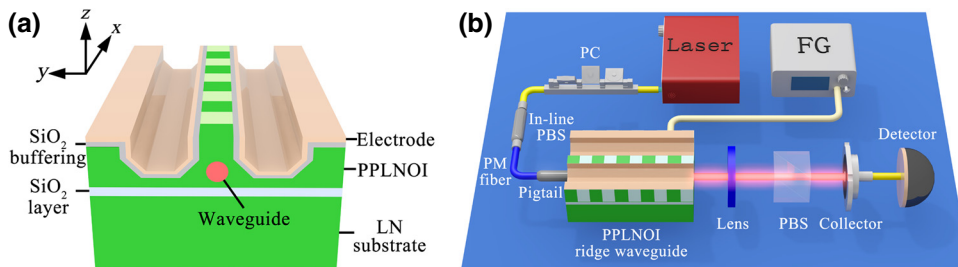


FIG. 1. (a) Cross-section view of the PPLNOI ridge waveguide. (b) Experimental setup of the integrated waveguide device for polarization control. FG: function generator; PC: polarization controller; PBS: polarization beam splitter; PM fiber: polarization maintaining fiber.

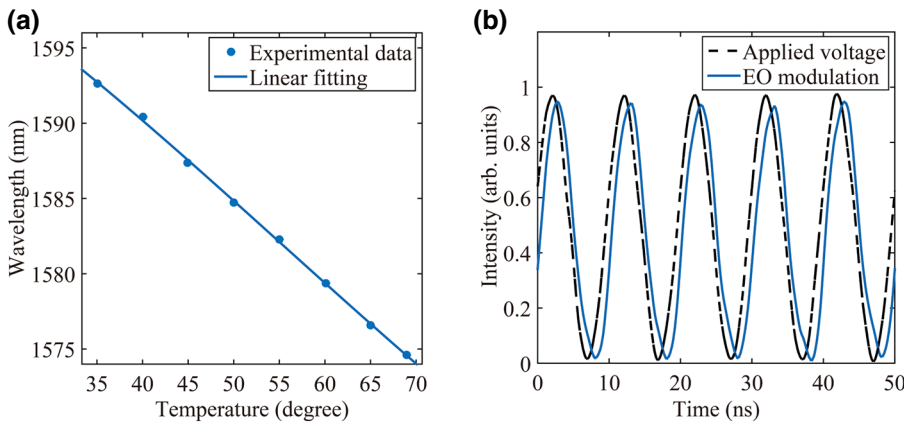


FIG. 2. (a) Experimentally measured QPM wavelength for EO coupling. (b) Experimental modulation of EO polarization coupling at a high speed of 100 MHz.

The experimental setup is depicted in Fig. 1(b). Light from a tunable continuous (cw) laser (1520–1600 nm) is used as the pump laser. A polarization controller (PC) is used to adjust its polarization. Light is injected into the integrated waveguide device, which includes an in-line polarized beam splitter (PBS), polarization maintain (PM) optical fiber with a pigtail end, a PPLNOI ridge waveguide, a function generator (FG), and a temperature controller with an accuracy of 0.1°C . The input light is kept TM polarized. The output is collimated by a short focal-length lens to free space, which is then injected into a detector after passing a PBS.

We first show the result of controlling the operating wavelength by adjusting the temperature of our device. Figure 2(a) shows the experimentally measured QPM wavelength for EO coupling, and the tuning slope is $-0.53\text{ nm}/^\circ\text{C}$. In practical applications, an excellent linear dependence of the operating wavelength on temperature is advantageous. We also measure the fast modulation rate of EO polarization coupling by applying a sinusoidal voltage of 100 MHz, as shown in Fig. 2(b). This shows the efficient mode conversion and the relatively high-speed operation capability of our device for EO coupling.

Then we demonstrate the linear polarization rotation characteristics of our device with efficient and linear EO

tuning. The operating wavelength is 1576.5 nm when the temperature is set at 65°C , and the output of PPLNOI is monitored by a polarimeter. The modulation of the output versus the applied voltage measured by the polarimeter is shown in Fig. 3(a). The half-wave voltage is approximately 7 V. Thus, the voltage-length product of our device is $7\text{ V} \cdot \text{cm}$. The performance has been improved from our previous version [26]. The presence of an offset angle at zero voltage can be attributed to the strain-optic effect, which can be easily compensated for by applying a balancing voltage. Figure 3(b) shows the polarization state of the output with respect to the applied voltage. A trajectory of the polarization evolution trajectory measured using the polarimeter is presented using the Poincaré sphere. As can be seen, the polarization well remains on the equatorial plane as the applied voltage varies, indicating the linear polarization at all rotation angles. It is measured that the rotation angle of the linearly polarized output has a good linear relationship with the applied voltage, which is consistent with theory.

To demonstrate the device's ability to control single-photon polarization states, we use the photon pairs generated from spontaneous parametric down-conversion (SPDC) other than weak coherent pulses. In the process of photon-pair generation, we use a 5-cm-long PPLN

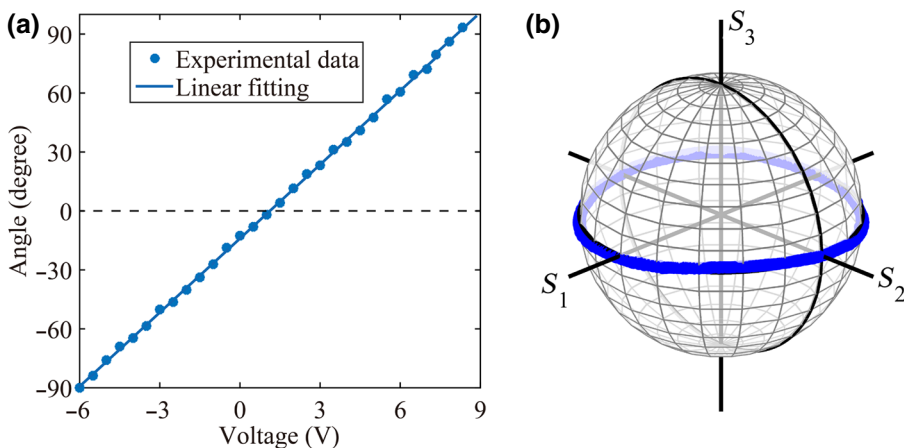


FIG. 3. (a) Rotation angle of the linearly polarized output varied with the applied voltage. (b) Output polarization state represented on a Poincaré sphere as the applied voltage varies.

waveguide with a poling period of $19.0\ \mu\text{m}$ to utilize the type-0 QPM scheme and its weak dispersion characteristics in the telecommunication band. As shown in Fig. 4(a), a TM-polarized 1557-nm cw laser amplified by an erbium-doped fiber amplifier is frequency doubled in a PPLN waveguide by second-harmonic generation (SHG). The 1557-nm fundamental laser in the output is suppressed by a wavelength division-multiplexing (WDM) with an extinction ratio of 180 dB and the 778.5-nm double-frequency component is launched into the second PPLN waveguide to serve as the pump for the SPDC process. The residual pump light (second-harmonic photons) and other fluorescence components are eliminated by another WDM with an extinction ratio of about 180 dB. The idler (1537.5 nm) and the signal (1576.5 nm) photons are then transferred to the corresponding dense wavelength-division multiplexing (DWDM) channels using a set of DWDM filters. The second PPLN is type-0 QPM, and the polarization of the pump light and two single photons are the same. The signal photons are injected into our device as mentioned before. After passing a lens and a PBS, the output signal photons are injected into a single-photon detector. On the other optical path, the idler single photons are injected into the other single-photon detector without any processing, except for increasing the delay with a long single-mode fiber.

Firstly, we remove the Mach-Zehnder interferometers (MZIs) in Fig. 4(a) to carry out EO linearly polarization coupling experiment of single photons. In this experiment, the photon-pair generation rate is set to 0.01 per detection gate. Each detection result is accumulated for 100 s with the dark count subtracted. The ability to control the single-photon polarization state can be observed by making coincidence counting measurements on single-photon detector 1 (SPD1) and SPD2 under different applied voltages. We set the orientation of the PBS so that only the TE or TM mode passes, and then measure the coincidence counting of the two single photons. The measured interference, as shown in Fig. 4(b), shows a clear sinusoidal relationship

with an average fitted visibility of $V = 96.3 \pm 2.65\%$, suggesting that our device can efficiently rotate the linear polarization state of single photons. The maintenance of its linear polarization state during the control of their polarization state can be inferred from the result as shown in Fig. 3.

In addition, another important feature of single-photon polarization switching is the maintenance of quantum properties during the conversion. This feature is demonstrated by measuring the quantum state visibility of the photon pairs before and after the mode conversion [27]. Time-energy entanglement between the two signal and idler photons [28] is measured, which is inherent in photon pairs generated via cw laser pumped SPDC. The time-energy entanglement can be demonstrated using Franson-type interferometry. We insert two unbalanced MZIs in front of the two SPDs, as shown in Fig. 4(a), and then implement a coincidence measurement. If the relative path delay between the two arms of the MZI is shorter than the coherence length of the cw laser, there will be no single-photon coherence fringe in the MZI's output, but a two-photon interference pattern will be observed by coincidence counting. The measured base vector can be changed by adjusting the phase of the long arm of the MZI. For example, the base vector of the signal single-photon is $|a\rangle + e^{i\theta}|b\rangle$, where θ represents the phase of the channel. a and b represent the long and short arms of the MZI, respectively. The state vector of the measurement basis rotates along the equator of the Poincaré sphere as θ changes. The coincidence count of the interference image can be estimated to be

$$N_c \propto 1 + V \cos(\theta_s + \theta_i - 2\omega_p \tau), \quad (3)$$

where V represents the visibility of the interference image. Subscripts p, s, i represent the pump, signal, and idler, respectively. τ represents the time corresponding to the optical path difference between the two paths of the MZI.

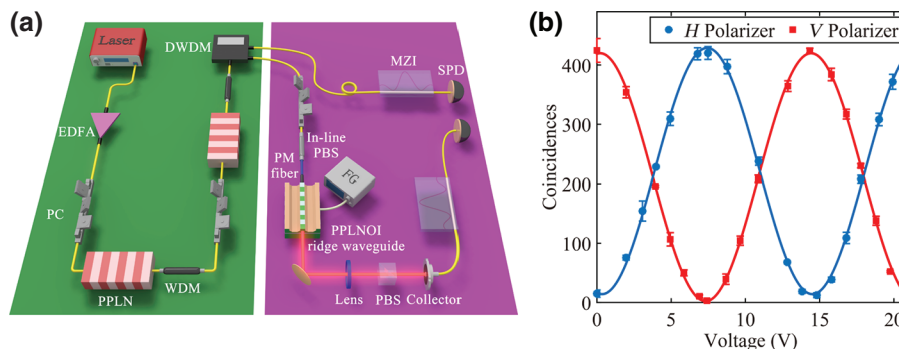


FIG. 4. (a) Schematic of single-photon generation and polarization control. (b) Coincidence count as a function of the voltage on the ridge waveguide. The blue and red lines indicate the PBS orientation that allows the single photon of the TE and TM modes to pass, respectively. PC, polarization controller; WDM, wavelength division-multiplexing; DWDM, dense wavelength-division multiplexing; PBS, polarization beam splitter; FG, function generator; MZI, unbalanced Mach-Zehnder interferometer; SPD, single-photon detector.

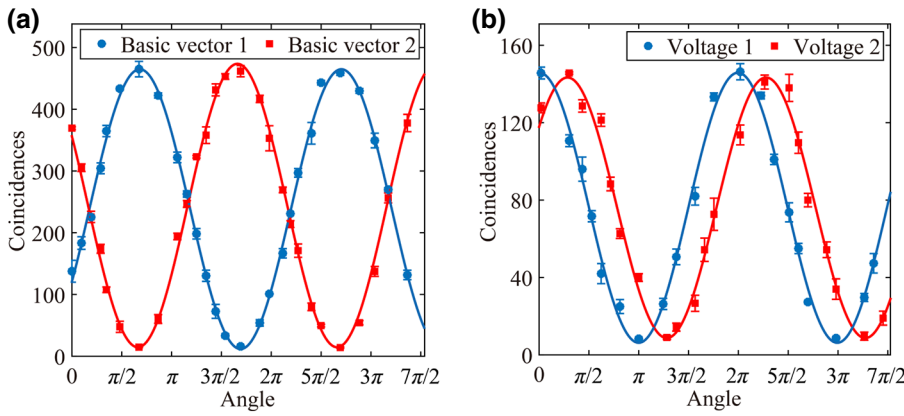


FIG. 5. Two-photon interference pattern (a) before and (b) after the polarization conversion. The integration time is (a) 10 s and (b) 50 s.

The theoretical visibility can be estimated by [29]

$$V = \frac{n\alpha_s\alpha_i}{n\alpha_s\alpha_i + 2(n\alpha_s + 2D_s)(n\alpha_i + 2D_i)}, \quad (4)$$

where n represents the mean photon-pair number per detection gate, which is 0.01 per gate in this experiment. $\alpha_{s,i}$ equals 10 dB, which is the loss from signal and idler channels, respectively. In addition, $D_s = D_i = 1 \times 10^{-6}$ is the dark count of each pulse gate. From Eq. (4) we can obtain a theoretical visibility of 98%.

In the experiment, the interference is obtained by changing the value of θ_i . We set the phase of the signal channel to two sets of noncollinear base vectors, and vary the phase of the idler channel, and the two-photon coincidence interference fringe pattern can be obtained. Figure 5(a) shows the interference pattern before the polarization control, and the average fitted visibility is $V = 94.5 \pm 0.53\%$. After the single-photon polarization controller, we measure the entanglement visibility of the converted photon pairs at different voltages, respectively, as shown in Fig. 5(b). The average fitted visibility is $V = 90.1 \pm 1.6\%$, which is beyond the 71% visibility necessary for the violation of the Bell inequality and thus excludes local realism from the quantum theory. The result convincingly shows that quantum correlation is well preserved during the polarization control. Thus, photon pairs after polarization control can still be used for quantum-communication tasks.

III. CONCLUSION

In conclusion, we demonstrate a linear polarization-state generator with a high precision based on the PPLNOI ridge waveguide structure. We succeed in controlling the polarization of single photons at the telecom wavelength via reduced voltage and high modulation rate by taking advantage of the LNOI platform and ridge-waveguide configuration. Moreover, the time-energy entanglement is well preserved during the control of the polarization state. The scheme holds promise for realizing integrated quantum optics.

ACKNOWLEDGMENTS

National Key R&D Program of China (2017YFA0303701, 2018YFA0306301); Shanghai Municipal Science and Technology Major Project (2019SHZDZX01); National Natural Science Foundation of China (NSFC) (11604206, 11734011); Foundation for Development of Science and Technology of Shanghai (17JC1400400); Shandong Quancheng Scholarship (00242019024).

- [1] J. O'Brien, A. Furusawa, and J. Vučković, Photonic quantum technologies, *Nat. Photonics*, **3**, 687 (2009).
- [2] S. Slussarenko and G. J. Pryde, Photonic quantum information processing: A concise review, *Appl. Phys. Rev.* **6**, 041303 (2019).
- [3] A. Boes, B. Corcoran, L. Chang, J. Bowers, and A. Mitchell, Status and potential of lithium niobate on insulator (LNOI) for photonic integrated circuits, *Laser Photonics Rev.* **12**, 1700256 (2018).
- [4] A. Christ, A. Eckstein, P. J. Mosley, and C. Silberhorn, Pure single photon generation by type-I PDC with backward-wave amplification, *Opt. Express* **17**, 3441 (2009).
- [5] M. Bock, A. Lenhard, C. Chunnillall, and C. Becher, Highly efficient heralded single-photon source for telecom wavelengths based on a PPLN waveguide, *Opt. Express* **24**, 23992 (2016).
- [6] M. F. Askarani, M. I. G. Puigibert, T. Lutz, V. B. Verma, M. D. Shaw, S. W. Nam, N. Sinclair, D. Oblak, and W. Tittel, Storage and reemission of heralded telecommunication-wavelength photons using a crystal waveguide, *Phys. Rev. Appl.* **11**, 054056 (2019).
- [7] A. Seri, G. Corrielli, D. Lago-Rivera, A. Lenhard, H. de Riedmatten, R. Osellame, and M. Mazzera, Laser-written integrated platform for quantum storage of heralded single photons, *Optica* **5**, 934 (2018).
- [8] T. Xiang, Q. C. Sun, Y. H. Li, Y. L. Zheng, and X. F. Chen, Single-photon frequency conversion via cascaded quadratic nonlinear processes, *Phys. Rev. A* **97**, 063810 (2018).
- [9] T. Guerreiro, A. Martin, B. Sanguinetti, J. S. Pelc, C. Langrock, M. M. Fejer, N. Gisin, H. Zbinden, N. Sangouard, and R. T. Thew, Nonlinear Interaction Between Single Photons, *Phys. Rev. Lett.* **113**, 173601 (2014).

- [10] C. E. Kuklewicz, M. Fiorentino, G. Messin, F. N. C. Wong, and J. H. Shapiro, High-flux source of polarization-entangled photons from a periodically poled KTiOPO₄ parametric down-converter, *Phys. Rev. A* **69**, 013807 (2004).
- [11] M. M. Weston, H. M. Chrzanowski, S. Wollmann, A. Boston, J. Ho, L. K. Shalm, V. B. Verma, M. S. Allman, S. W. Nam, R. B. Patel, S. Slussarenko, and G. J. Pryde, Efficient and pure femtosecond-pulse-length source of polarization-entangled photons, *Opt. Express* **24**, 10869 (2016).
- [12] C. W. Sun, S. H. Wu, J. C. Duan, J. W. Zhou, J. L. Xia, P. Xu, Z. D. Xie, Y. X. Gong, and S. N. Zhu, Compact polarization-entangled photon-pair source based on a dual-periodically-poled Ti : LiNbO₃ waveguide, *Opt. Lett.* **44**, 5598 (2019).
- [13] G. B. Xavier, G. Vilela de Faria, G. P. Temporão, and J. P. von der Weid, Full polarization control for fiber optical quantum communication systems using polarization encoding, *Opt. Express* **16**, 1867 (2008).
- [14] Y. Y. Ding, W. Chen, H. Chen, C. Wang, Y. P. Li, S. Wang, Z. Q. Yin, G. C. Guo, and Z. F. Han, Polarization basis tracking scheme for quantum key distribution with revealed sifted key bits, *Opt. Lett.* **42**, 1023 (2016).
- [15] X. D. Cai, D. Wu, Z. E. Su, M. C. Chen, X. L. Wang, L. Li, N. L. Liu, C. Y. Lu, and J. W. Pan, Entanglement-based Machine Learning on a Quantum Computer, *Phys. Rev. Lett.* **114**, 110504 (2014).
- [16] D. Bonneau, M. Lobino, P. Jiang, C. M. Natarajan, M. G. Tanner, R. H. Hadfield, S. N. Dorenbos, V. Zwiller, M. G. Thompson, and J. L. O'Brien, Fast Path and Polarization Manipulation of Telecom Wavelength Single Photons in Lithium Niobate Waveguide Devices, *Phys. Rev. Lett.* **108**, 053601 (2012).
- [17] H. Jin, F. M. Liu, P. Xu, J. L. Xia, M. L. Zhong, Y. Yuan, J. W. Zhou, Y. X. Gong, W. Wang, and S. N. Zhu, On-chip Generation and Manipulation of Entangled Photons Based on Reconfigurable Lithium-Niobate Waveguide Circuits, *Phys. Rev. Lett.* **113**, 103601 (2014).
- [18] J. W. Wang, A. Santamato, P. Jiang, D. Bonneau, E. Engin, J. Silverstone, M. Lerner, J. Beetz, M. Kamp, S. Höfling, M. Tanner, C. Natarajan, R. Hadfield, S. Dorenbos, V. Zwiller, J. O'Brien, and M. Thompson, Gallium arsenide (GaAs) quantum photonic waveguide circuits, *Opt. Commun.* **327**, 49 (2014).
- [19] N. Zeng, X. Y. Jiang, Q. Gao, Y. H. He, and H. Ma, Linear polarization difference imaging and its potential applications, *Appl. Opt.* **48**, 6734 (2009).
- [20] A. Kuhn, M. Hennrich, and G. Rempe, Deterministic Single-Photon Source for Distributed Quantum Networking, *Phys. Rev. Lett.* **89**, 067901 (2002).
- [21] W. T. Liao, A. Pálffy, and C. H. Keitel, Coherent Storage and Phase Modulation of Single Hard-x-ray Photons Using Nuclear Excitons, *Phys. Rev. Lett.* **109**, 197403 (2012).
- [22] J. Capmany and C. R. Fernández-Pousa, Spectral decomposition of single-tone-driven quantum phase modulation, *J. Phys. B: At. Mol. Opt. Phys.* **44**, 035506 (2011).
- [23] N. Courjal, B. Guichardaz, G. Ulliac, J.-Y. Rauch, B. Sadani, H. Lu, and M.-P. Bernal, High aspect ratio lithium niobate ridge waveguides fabricated by optical grade dicing, *J. Phys. D: Appl. Phys.* **44**, 305101 (2011).
- [24] M. F. Volk, S. Suntsov, C. E. Rüter, and D. Kip, Low loss ridge waveguides in lithium niobate thin films by optical grade diamond blade dicing, *Opt. Express* **24**, 1386 (2016).
- [25] K. Liu, J. H. Shi, and X. F. Chen, Linear polarization-state generator with high precision in periodically poled lithium niobate, *Appl. Phys. Lett.* **94**, 101106 (2009).
- [26] T. T. Ding, Y. L. Zheng, and X. F. Chen, On-chip solc-type polarization control and wavelength filtering utilizing periodically poled lithium niobate on insulator ridge waveguide, *J. Lightwave Technol.* **37**, 1296 (2019).
- [27] Q. Zhang, H. Takesue, S. W. Nam, C. Langrock, X. P. Xie, B. Baek, M. M. Fejer, and Y. Yamamoto, Distribution of time-energy entanglement over 100 km fiber using superconducting single-photon detectors, *Opt. Express* **16**, 5776 (2012).
- [28] J. D. Franson, Bell Inequality for Position and Time, *Phys. Rev. Lett.* **62**, 2205 (1989).
- [29] J. F. Dynes, H. Takesue, Z. L. Yuan, A. W. Sharpe, K. Harada, T. Honjo, H. Kamada, O. Tadanaga, Y. Nishida, M. Asobe, and A. J. Shields, Efficient entanglement distribution over 200 kilometers, *Opt. Express* **17**, 11440 (2009).